Analysis of rotor fault detection in inverter fed induction machines at no load by means of finite element method

M.A. Samonig, P. Nussbaumer, G. Stojicic, Th.M. Wolbank
Department of Electrical Drives and Machines
Vienna University of Technology
thomas.wolbank@tuwien.ac.at

Abstract- **This paper analyzes a new method for detecting defective rotor bars at zero load and standstill by means of modeling using the finite element method (FEM). The detection method uses voltage pulses generated by the switching of the inverter to excite the machine and measures the corresponding reaction of the machine phase currents, which can be used to identify a modulation of the transient leakage inductance caused by asymmetries within the machine. The presented 2D finite element model and the simulation procedure are oriented towards this approach and are developed by means of the FEM software ANSYS. The analysis shows how the transient flux linkage imposed by voltage pulses is influenced by a broken bar leading to very distinct rotor-fixed modulation, that can be clearly exploited for monitoring. Simulation results are presented to show the transient flux paths. These simulation results are supported by measurements on a specially manufactured induction machine.**

I. Introduction

In modern drives applications reliability considerations are becoming increasingly important. Although induction machines (IM) are presumed as considerably robust, they have to cope with increased stress, especially in controlled mode and with repeated load cycles. According to studies, a considerable percentage of all breakdowns is caused by defects in the rotor cage [1]-[3].

A wide range of different fault detection methods has already been published [4]. Most of these approaches are limited to mains fed machines and apply current signature analysis (CSA) to identify side bands in the stator current used as fault indicators. To determine these indicators different analysis methods are used. Examples are wavelet transform [5],[6], Fourier transform [7],[8], Hilbert transform [9], pattern recognition [10] or neural network approaches [11],[12]. Genetic algorithms can be used to account for the fault indicator's load dependence [13].

Although methods based on or closely related to CSA work well for mains fed machines in combination with changing load levels, they are usually limited to quasi-steady state operating conditions in terms of inverter feeding. The investigation in [4] deals with fault indicators introduced by torque pulsations, [14] uses Wigner distribution to allow operation at changing stator frequency (10Hz/sec). In [15] and [16] the stator current phasor is considered in a synchronous reference frame to eliminate its dependence on the fundamental wave frequency, which otherwise is masking the fault indicator comprising two slip-related side bands.

By comparing the torque calculated from the stator and rotor equation respectively and clustering the data along the rotor angle a fault indicator can be determined by means of fundamental wave models [17]. Virtual current is used in [18] to identify rotor defects.

An essential requirement regarding rotor fault detection with all the methods mentioned above is a minimum load level of about 30% - 40%. The following methods can be used at zero load. The methods proposed in [19]-[22] are injecting rotating and pulsating signals at standstill respectively. The method presented in [23] identifies the rotor time constant in different spatial directions, however not at standstill, as a specific rotor speed has to be maintained.

In [24] a new method for fault detection of inverter-fed induction machines was proposed. It is applicable at zero load and standstill and uses the inverter to excite the machine's phases with a sequence of voltage pulses. By measuring the transient current responses with the built-in current sensors, asymmetries within the machine are detectable as they cause a modulation of the machine's transient stator inductance that also occurs in the stator currents. Analysis of this modulation allows for the extraction of a fault indicator.

Transient voltage pulses of some 10µs duration form the base of this detection method. FEM analysis of rotor bar faults so far was limited to sinusoidal excitation and the results are thus not applicable for a detailed investigation. In order to illustrate the changes in the flux linkage associated to the transient excitation as well as to analyze the applicability of the proposed fault detection method to different machine designs, this paper describes a possible modeling approach featuring the FEM-software ANSYS.

II. Fault Detection At Standstill Without Fundamental Wave Excitation

This chapter summarizes the most important aspects of the fault detection method proposed in [24]. Considerations start with the stator equation (1).

$$\underline{v}_S = r_S \cdot \underline{i}_S + l_l \cdot \frac{d\underline{i}_S}{d\tau} + \frac{d\underline{\lambda}_R}{d\tau} \qquad (1)$$

978-1-61284-971-3/11/$26.00 ©2011 IEEE

The stator (index S) voltage phasor $\underline{v}_S$ comprises several parts: the voltage drop impressed by the stator current phasor $\underline{i}_S$ on the stator resistance r_S, the voltage due to the change of the stator current $d\underline{i}_S/d\tau$ in the leakage (index l) inductance l_l and the time derivative of the rotor (index R) flux $\underline{\lambda}_R$ (back emf).

If the machine's phases are excited by voltage pulses the value of the leakage inductance effective differs from that for the fundamental wave, what leads to the introduction of the transient (index t) leakage inductance $l_{l,t}$ in the following. For an excitation with a positive (index I) and negative (index II) voltage pulse equation (1) can be written as (2) and (3) respectively.

$$\underline{v}_{S,I} = r_S \cdot \underline{i}_{S,I} + l_{l,t} \cdot \frac{d\underline{i}_{S,I}}{d\tau} + \frac{d\underline{\lambda}_{R,I}}{d\tau} \tag{2}$$

$$\underline{v}_{S,II} = r_S \cdot \underline{i}_{S,II} + l_{l,t} \cdot \frac{d\underline{i}_{S,II}}{d\tau} + \frac{d\underline{\lambda}_{R,II}}{d\tau} \tag{3}$$

For an ideal, perfectly symmetrical machine, the transient leakage inductance $l_{l,t}$ would be a scalar. In reality though, a machine never is completely symmetrical. There are always asymmetries imposed by its geometry (e.g. rotor/stator slotting) and even more important by machine faults (e.g. broken rotor bars or eccentricities). Such asymmetries cause a variation of the transient leakage inductance along the machine's air gap and therefore have an influence on the resulting current change in the machine's phases. This influence can be described by introducing a complex transient leakage inductance $\underline{l}_{l,t}$, (4) consisting of the constant (index *const*) part l_{const} and a modulation (index *mod*) with the amplitude l_{mod}, which is dependent on the spatial position γ of the maximum inductance within one pole pair.

$$\underline{l}_{l,t} = l_{const} + l_{\mathrm{mod}} \cdot e^{j2\gamma} \tag{4}$$

The next step towards the desired fault asymmetry signal is the subtraction of equations (2) and (3) to eliminate the influence of the voltage drop imposed on the stator resistance and the back emf, which yields (5).

$$\underline{v}_{S,I} - \underline{v}_{S,II} = \underline{l}_{l,t}\left(\frac{d\underline{i}_{S,I}}{d\tau} - \frac{d\underline{i}_{S,II}}{d\tau}\right) = \underline{l}_{l,t}\left(\frac{d\underline{i}_{S,I-II}}{d\tau}\right) = \underline{v}_{S,I-II} \tag{5}$$

This step is perfectly valid for a machine at standstill ($\underline{i}_S$=0, $\underline{\lambda}_S$=0) without fundamental wave excitation but is still useable for a rotating, energized machine if the changes of the stator current phasor and the back emf between the positive and negative voltage pulse are negligible. The corresponding approximations are given in (6), where also the time derivative of the current is approximated by the difference Δ.

$$\underline{i}_{S,I} \approx \underline{i}_{S,II}, \quad \frac{d\underline{\lambda}_{R,I}}{d\tau} \approx \frac{d\underline{\lambda}_{R,II}}{d\tau} \text{ and } \frac{d\underline{i}_S}{d\tau} \approx \frac{\Delta\underline{i}_S}{\Delta\tau}. \tag{6}$$

Inverting (5) yields,

$$\frac{\Delta\underline{i}_{S,I-II}}{\Delta\tau} = y_{const} \cdot \underline{v}_{S,I-II} + \underline{y}_{\mathrm{mod}} \cdot \underline{v}_{S,I-II} = \underline{y} \cdot \underline{v}_{S,I-II}. \tag{7}$$

The variable $\underline{y}$ contains the whole information on the asymmetries within the machine and can be used to extract a fault indicator for broken rotor bars. Fig. 1 illustrates the relationship stated by (7) for a transient pulse excitation in the direction of the machine's phase U (real axis). Dependent on the angular position γ of the maximum inductance within one pole pair, the tip of the current change phasor $\Delta\underline{i}_{S,I-II}/\Delta\tau$ moves along the dashed circle line. As can be seen, the difference of the applied two voltage phasors $\underline{v}_{S,I-II}$ and the resulting current slope no longer share the same direction. This is a consequence of the complex variable $\underline{y}$ representing the machine's asymmetries.

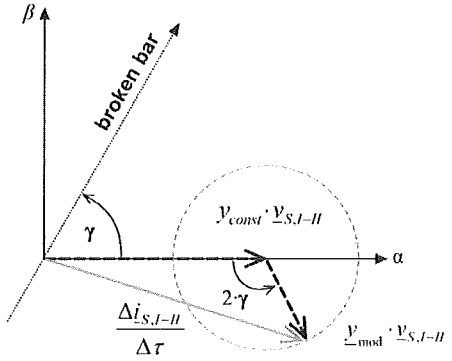

Fig. 1. Dependence of current slope $\Delta\underline{i}_S/\Delta\tau$ on the spatial angle γ for an applied voltage phasor $\underline{v}_S$ in direction of phase U.

III. Modeling And Simulation Approach

This chapter presents the model used for fault detection simulations on a demagnetized squirrel cage induction machine at standstill (note that the test machine in [24] was not demagnetized). The model was created with ANSYS Parametric Design Language (APDL), which is a scripting language. It offers a wide range of commands that can be used to write macro codes to automate tasks and parameterize the model. Parameterization is very useful when it comes to the simulation of different machine designs as it allows for the easy change of machine parameters.

With regard to the model the most important specifications of the experimental IM are listed in TABLE I.

TABLE I
Experimental Machine Specifications

Stator	Rotor
36 slots	28 slots
Two layer 7/9 fractional pitch winding (9 turns per coil)	Unskewed squirrel cage
3 phases (U, V, W)	Copper bars
4 poles	-
Wye connected (Y)	-

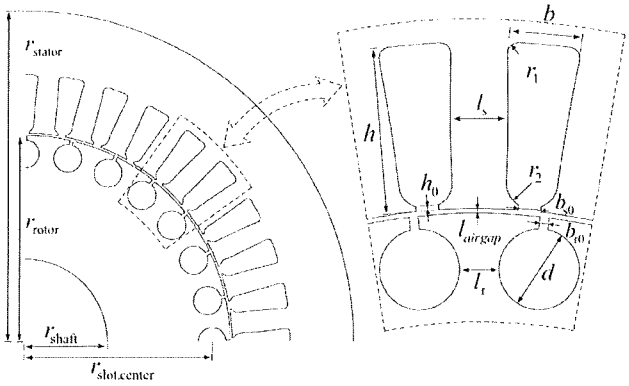

Fig. 2. Geometric model

A. Geometric Model

For the presented model a bottom-up approach is selected, i.e. modeling starts with the generation of keypoints, which represent the lowest geometric layer.

In the second step two keypoints at a time are connected by one line. For the given machine this results in a grid somewhat like the one shown in Fig. 2. Note that only one fourth of the given machine is displayed. The figure also shows the used geometric parameters.

In step three the lines are used as borders to generate areas, which represent the topmost layer in a 2D model. (A 3D model would pass on to the next layer, i.e. volumes bordered by areas.)

If a top-down approach is appreciated the APDL commands can be used to start with the generation of areas followed by operations to modify these areas, like Boolean operations that add or subtract them. In this case all subsidiary layers will be generated automatically.

B. Property Allocation and Meshing

The areas assembling the geometry represent the different parts of the IM: the rotor shaft, body, bars and slot openings, the air gap and the stator body, windings and slot openings. The materials used are: copper, air and grain-oriented electrical sheet (M800-50A). These three materials are assigned to the corresponding areas in addition to a finite element type usable for a 2D transient electromagnetic simulation. The elements applied can have up to 4 degrees of freedom (DOF) in each of their 8 nodes. The element's geometry and the DOF are shown in Fig. 3.

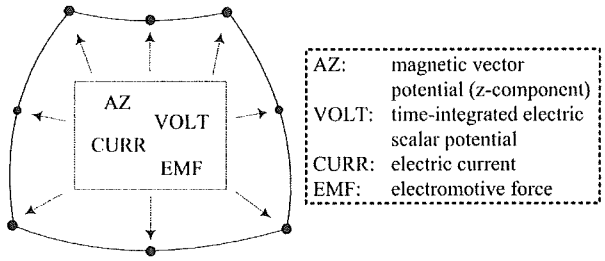

Fig. 3. Finite element used for domains of TABLE II.

The actual number of DOF per node has to be adjusted depending on the model region the element is assigned to. TABLE II lists the different domains and the associated DOF.

TABLE II
DIFFERENT FINITE ELEMENT DOMAINS

Domain	Material	Element use	DOF
Stator/rotor body	M800-50A	static domain	AZ
Air regions	Air	static domain	AZ
Stator winding	Copper	circuit-coupled stranded coil	AZ, CURR, EMF
Rotor bars	Copper	circuit-coupled massive conductor	AZ, CURR, EMF

After assignment of the material and element type to the areas, the model is ready for meshing. For this purpose the automatic meshing is used to generate two separate meshes, one for the rotor and the other one for the stator areas. The boundary between these two domains is laid into the middle of the air gap and a sliding interface is established to couple the separate meshes physically.

As can be seen in TABLE II the stator winding and rotor elements are coupled to circuits. These circuits are composed of circuit elements. Similar to the element of Fig. 3 they can fulfill different functions that are listed in TABLE III. Each of the coil and conductor circuit elements has to be associated to the corresponding finite element domain represented by a meshed area, as shown in Fig. 4. To model the squirrel cage the rotor bar circuit elements are connected in parallel by coupling the VOLT DOF at both ends. One stator phase is composed of 24 stranded coil elements (two for a full coil) and an independent voltage source connected in series. The three phases are connected in parallel as pictured in Fig. 4.

TABLE III
USED CIRCUIT ELEMENTS

Circuit element	DOF
Independent voltage source	VOLT, CURR
Stranded coil	VOLT, CURR, EMF
Massive conductor	VOLT, CURR, EMF

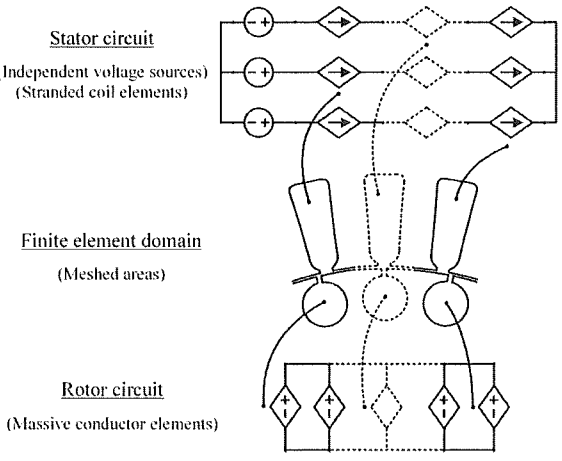

Fig. 4. Schematic diagram of stator/rotor circuit and corresponding finite element domains.

C. Simulation

As stated above already, (7) is perfectly valid for a demagnetized IM at standstill and can be used as done in [24] or [25]. There are though two differences compared to the pulsed excitation used for the measurements.

1. No complete voltage pulse sequence but only one voltage step is simulated.
2. Separate simulations are carried out for the positive and negative voltage step.

Fig. 5 shows the excitation and corresponding current response for a positive voltage step.

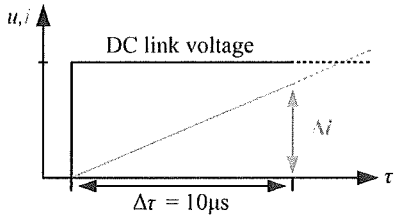

Fig. 5. Current response due to an excitation by a voltage step.

In fact, simulation of the negative voltage pulse can be omitted if the results of the positive pulse are inverted. But to stay as close as possible to the procedures of [24] and [25] and with respect to future simulations for a rotating machine negative pulses were simulated too. The actual simulation procedure is as follows:

1. Application of a voltage step in direction of phase U with duration of 10μs.
2. Saving the simulation results.
3. Moving the rotor by a given angle (dependent on the resolution necessary).
4. Starting a separate simulation for the new rotor position with step 1.

This sequence is repeated in a loop until the rotor reaches its end position after one angular period. In a separate tread the corresponding current changes are calculated per phase from the stored results and transferred to MATLAB for further analysis. The next chapter presents results obtained from this analysis.

IV. Results

Due to the 2D-modelling and the approximation of the transient magnetic properties there is a difference detectable between the simulated and measured current slope. As will be shown in this chapter, the ratio between the different inherent modulations however shows good agreement between simulation and measurement.

A. Faultless Rotor

Fig. 6 shows the flux line plot for a voltage excitation in direction of phase U. As the machine comprises four poles the voltage step causes positive excitations in the directions denoted $+U$ and negative ones in the directions $-U$. Since the squirrel cage is faultless it prevents the transient magnetic field from penetrating the rotor especially beneath the bars by presenting a current linkage in the rotor bars opposing that of the stator winding. In other words, due to the fact that the rotor time constant τ_R (344ms) is several orders higher than the duration of the applied voltage step (10μs) the transient flux is restricted to the rotor surface. As shown in Fig. 6 the dominant part of this transient rotor flux is the zigzag flux that crosses the air gap and alternates between stator and rotor avoiding the wide stator slot openings.

Turning the rotor for a total of 360° (one mechanical revolution) using the sequence presented above yields the spectrum depicted in Fig. 8. The figure shows the 28th harmonic as the dominant spectral line. It is called slotting harmonic because it originates directly from the 28 rotor slots and is the major source of asymmetry in the given case. Fig. 10 shows the spectrum obtained from measurements for a faultless test machine for the same operating conditions. It has to be noted that the test IM in this case was not demagnetized and that the vertical axis has been rescaled for comparison reasons. Compared to the simulation results the measured spectrum contains several additional harmonics. The most important are described in the following. Since a machine in reality is never completely symmetrical, inherent asymmetries besides the slotting harmonic (like rotor eccentricities) introduce a 4th harmonic due to the fact that the given IM has four poles.

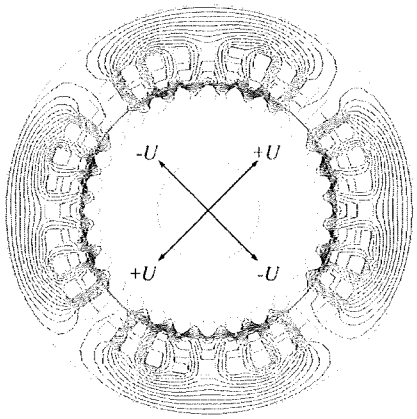

Fig. 6. Flux line plot for a positive voltage excitation of a faultless IM. $\pm U$ give the directions of excitation representing the four poles.

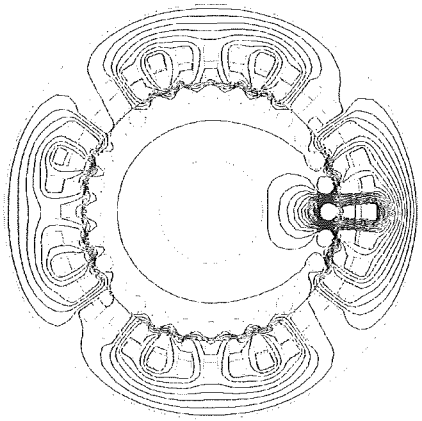

Fig. 7. Flux line plot for a positive voltage excitation of an IM with one broken rotor bar.

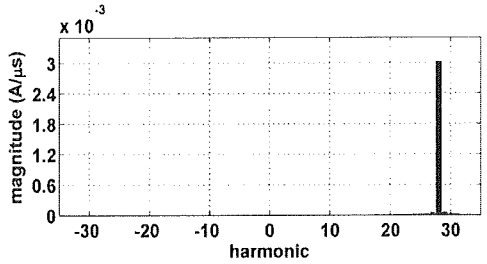

Fig. 8. Spectrum of the asymmetry phasor determined from simulation of a demagnetized faultless IM for one mechanical revolution.

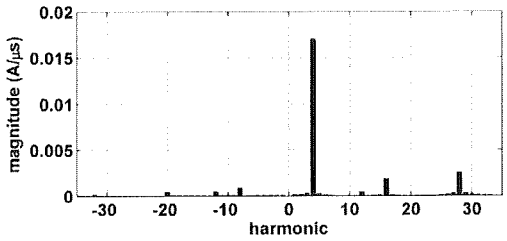

Fig. 9. Spectrum of the asymmetry phasor determined from simulation of a demagnetized IM with a broken rotor bar for one mechanical revolution.

Additional information on the 4th harmonic can be found in the next section. The -32th harmonic originates from an intermodulation of the 28th and the mentioned 4th harmonic. Finally the -28th harmonic represents the influence of other inherent asymmetries on the slotting harmonic.

B. Broken Rotor Bar

In another set of simulations a fully broken bar was introduced in one of the rotor slots. This is achievable in two different ways, first by increasing the corresponding bar's resistance or secondly by assigning air as the material property of the corresponding rotor bar area. For the results presented the latter approach has been employed. Fig. 7 depicts the simulation results represented as flux line plot for the transient excitation of the given IM model. The broken rotor bar represents a weak spot in the squirrel cage and allows for a deeper penetration of the transient flux into the rotor body. Thus, the rotor slot opening can be bypassed underneath the defective bar. As a consequence the symmetrical flux distribution of Fig. 6 is disturbed, which is accompanied by asymmetry in the machine's transient current response of the three phases. Repeating the simulation for different angular rotor positions leads to a modulation in this asymmetric phase currents and the corresponding current phasor slope. For a full mechanical revolution this results in the 4th harmonic of Fig. 9. The 4th order of this harmonic is a consequence of the 4 machine poles, as the broken bar experiences 4 equivalent flux conditions (independent of the sign of the flux) during a 360° revolution. Fig. 11 shows the rescaled spectrum obtained from measurements on a test machine with one broken rotor bar for the same operating conditions. Obviously the results of simulation and measurement are in good agreement.

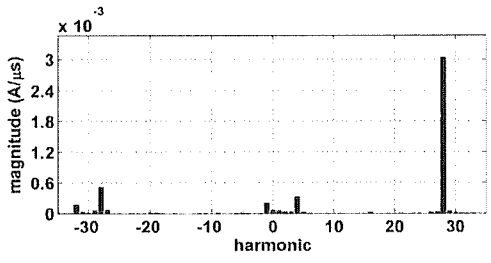

Fig. 10. Spectrum of the asymmetry phasor determined from measurements on a faultless IM (not demagnetized) for one mechanical revolution. (Rescaled vertical axis).

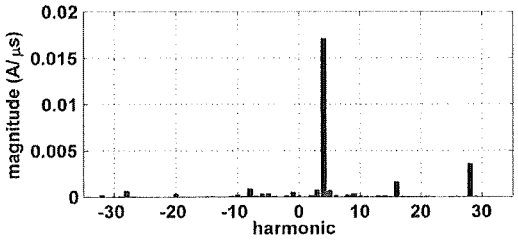

Fig. 11. Spectrum of the asymmetry phasor determined from measurements on an IM (not demagnetized) with a broken rotor bar for one mechanical revolution. (Rescaled vertical axis).

C. Closed Rotor Slots

A primal motivation for modeling the test IM by means of the FEM was to carry out simulations for different machine designs and analyze their effect on the asymmetry spectrum especially on the 4th harmonic used as fault indicator. One of these special design cases is represented for example by a machine with closed rotor slots. To simulate these conditions the presented model has been modified by assigning magnetic material (M800-50A) instead of air to the rotor slot openings. The simulation process remained the same as described in the previous section.

The simulation results for the faultless (symmetrical) rotor showed a 28th harmonic with a magnitude of 1.88e-6. This is a decrease of 3 orders of magnitude (10^{-3}) compared to that of the open slot machine (Fig. 8). This decrease is due to the fact that a considerable part of the transient zigzag flux no longer has to avoid the rotor slot openings by passing the air gap and therefore is independent of the rotor position. As a consequence the rotor slot harmonic no longer is detectable as it can not be distinguished from random noise in the measurement results. However this is not critical for the analyzed fault detection method where the 4th harmonic is used as fault indicator. The resulting spectrum for a broken rotor bar and closed rotor slots is shown in Fig. 12. As already stated above the dominant spectral line introduced by a broken rotor bar is the 4th harmonic. In the case under consideration its magnitude is two orders (10^{-2}) smaller than the one shown for open rotor slots (Fig. 9). However, the accuracy of the measurement procedure is extremely high. In [25] an increase in resistance of a single bar of only 13% was proven to be reliable detectable. It can thus be assumed that the detection of a broken bar is still possible in such machine design.

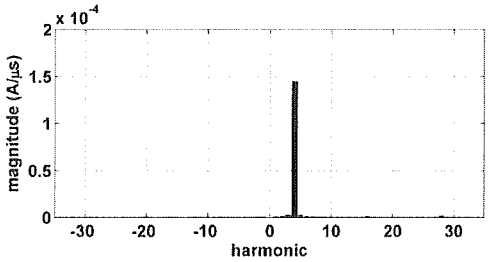

Fig. 12. Spectrum of the asymmetry phasor determined from simulation of a demagnetized IM with one broken rotor bar and closed rotor slots for one mechanical revolution.

V. CONCLUSIONS

A FEM analysis of a method to detect rotor faults in inverter-fed induction machines was presented. The model is built in the FEM software ANSYS by means of a parametric design language that allows for an easy adjustable model to simulate the effect of different machine geometries on the given fault detection method. As the rotor fault detection method excites the machine with voltage pulses of some 10μs duration a transient simulation is needed to simulate the effect of asymmetries within the machine on the phase current slopes. A major source of asymmetry in squirrel cage induction machines is represented by broken rotor bars. It was shown that a broken bar leads to a local asymmetry in the spatial distribution of the transient flux that can be detected and used for detection of rotor bar defects. A comparison of the FEM simulation with measurement results showed good agreement especially regarding the 4th harmonic used as fault indicator. To extend the results to different machine designs an analysis was performed on machines with closed rotor slot design based on FEM simulation. Though the magnitude of the fault indicator harmonic is then clearly reduced the detection of a broken bar is still possible due to the high accuracy of the method.

REFERENCES

[1] IEEE Committee Report, "Report of large motor reliability survey of industrial and commercial installation, Part I and Part II," *IEEE Trans. Industry Applications*, vol.21, no.4, pp.853–872, 1985

[2] P. F. Albrecht, J. C. Appiarius and D. K. Sharma, "Assessment of the reliability of motors in utility applications—Updated," *IEEE Trans. Energy Conversions*, vol.1, no.1, pp.39–46, 1986

[3] A. H. Bonnet and C. Yung, "Increased efficiency versus increased reliability," *IEEE Industry Applications Magazine* vol.14, no.1, pp.29-36, 2008.

[4] A. Bellini, F. Filippetti, C. Tassoni and G. Capolino, "Advances in Diagnostic Techniques for Induction Machines," *IEEE Trans. Industrial Electronics*, vol.55, no.12, pp.4109-4126, 2008

[5] S.H. Kia, H. Henao and G. Capolino, "Diagnosis of Broken Bar Fault in Induction Machines Using Discrete Wavelet Transform without Slip Estimation," *IEEE Trans. Industry Applications*, vol.45, no.4, pp.1395-1404, 2009

[6] A. Ordaz-Moreno, R. de Jesus Romero-Troncosos, J. A. Vite-Frias, J. R. Rivera-Gillen and A. Garcia-Perez, "Automatic Online Diagnosis Algorithm for Broken-Bar Detection on Induction Motors Based on Discrete Wavelet Transform for FPGA Implementation," *IEEE Trans. Industrial Electronics*, vol.55, no.12, pp.2193-2202, 2008

[7] W. Le Roux, R. G. Harley and T. G. Habetler, "Detecting Rotor Faults in Low Power Permanent Magnet Synchronous Machines," *IEEE Trans. Power Electronics*, vol.22, no.1, pp.322-328, 2007

[8] A. Khezzar, M. Y. Kaikaa, M. E. K. Oumaamar, M. Boucherma and H. Razik, "On the Use of Slot Harmonics as a Potential Indicator of Rotor Bar Breakage in the Induction Machine," *IEEE Trans. Industrial Electronics*, vol.56, no.11, pp.4592-4605, 2009

[9] M. Pineda-Sanchez, M. Riera-Guasp, J. A. Antonino-Daviu, J. Roger-Folch, J. Perez-Cruz and R. Puche-Panadero, "Instantaneous Frequency of the Left Sideband Harmonic During the Start-Up Transient: A New Method for Diagnosis of Broken Bars," *IEEE Trans. Industrial Electronics*, vol.56, no.11, pp.4557-4570, 2009

[10] M. Haji and H. A. Toliyat, "Pattern Recognition - a Technique for Induction Machines Rotor Fault Detection eccentricity and Broken Bar Fault," *Proc. Industry Applications Annual Conference IAS*, vol.3, pp.1572-1578, 2001

[11] B. Ayhan, M.-Y. Chow and M.-H. Song, "Multiple Discriminant Analysis and Neural-Network-Based Monolith and Partition Fault-Detection Schemes for Broken Rotor Bar in Induction Motors," *IEEE Trans. Industrial Electronics*, vol.53, no.4, pp.1298-1308, 2006

[12] F. Filippetti, G. Franceschini and C. Tassoni, "Neural networks aided on-line diagnostics of induction motor rotor faults," *IEEE Trans. Industry Applications*, vol.31, no.4, pp.892-899, 1995

[13] H. Razik, M. B. de Rossiter Corrêa and E. R. C. da Silva, "A Novel Monitoring of Load Level and Broken Bar Fault Severity Applied to Squirrel-Cage Induction Motors Using a Genetic Algorithm," *IEEE Trans. Industrial Electronics*, vol.56, no.11, pp.4615-4626, 2009

[14] M. Blödt, D. Bonacci, J. Regnier, M. Chabert and J. Faucher, "On-Line Monitoring of Mechanical Faults in Variable-Speed Induction Motor Drives Using the Wigner Distribution," *IEEE Trans. Industrial Electronics*, pp.522-531, 2008

[15] S. M. A. Cruz and A. J. Marques Cardoso, "Rotor Cage Fault Diagnosis in Three-Phase Induction Motors, by Extended Park's Vector Approach," *Proc. International Conference on Electrical Machines*, pp.1844-1848, 1998

[16] S. M. A. Cruz, H. A. Toliyat and A. J. Marques Cardoso, "DSP implementation of the multiple reference frames theory for the diagnosis of stator faults in a DTC induction motor drive," *IEEE Trans. Energy Conversion*, pp.329-335, 2005

[17] C. Kral, F. Pirker, G. Pascoli and H. Kapeller, "Robust Rotor Fault Detection by Means of the Vienna Monitoring Method and a Parameter Tracking Technique," *IEEE Trans. Industrial Electronics*, vol.55, no.12, pp. 4229-4237, 2008

[18] S. M. Cruz, A. Stefani, F. Filippetti and A. J. Marques Cardoso, "A New Model-Based Technique for the Diagnosis of Rotor Faults in RFOC Induction Motor Drives," *IEEE Trans. Industrial Electronics*, vol.55, no.12, pp.4218-4228, 2008

[19] S. B. Lee, J. Yang, J. Hong, B. Kim, J. Yoo, K. Lee, J. Yun, M. Kim, K. Lee, E. J. Wiedenbrug, and S. Nandi, "A New Strategy for Condition Monitoring of Adjustable Speed Induction Machine Drive Systems," *Proc. IEEE International Symposium on Diagnostics for Electric Machines, Power Electronics and Drives, SDEMPED*, pp.1-9, 2009

[20] B. Kim, K. Lee, J. Yang, S. B. Lee, E. Wiedenbrug and M. Shah, "Automated detection of rotor faults for inverter-fed induction machines under standstill conditions," *IEEE Energy Conversion Congress and Exposition*, pp.2277-2284, 2009

[21] C. Concari, G. Franceschini and C. Tassoni, "Self-commissioning procedures to detect parameters in healthy and faulty induction drives," *Proc. IEEE International Symposium on Diagnostics for Electric Machines, Power Electronics and Drives, SDEMPED*, pp.1-6, 2009

[22] B. Akin, A. B. Ozturk, H. A. Toliyat and M. Rayner, "DSP-Based Sensorless Electric Motor Fault-Diagnosis Tools for Electric and Hybrid Electric Vehicle Powertrain Applications," *IEEE Trans. Vehicular Technology*, vol.58, no.6, 2679-2688, 2009

[23] T. Wolbank, J. Machl, R. Schneiderbauer, "Detecting Rotor Faults in Inverter-Fed Induction Machines at Zero Load," *Proc. International Power Electronics and Motion Control Conference, EPE-PEMC*, Riga, Latvia, pp.1-6, 2004

[24] Th.M. Wolbank, P. Nussbaumer, H. Chen and P.E. Macheiner, "Monitoring of Rotor Bar Defects in Inverter-Fed Induction Machines at Zero Load and Speed," *IEEE Trans. Industrial Electronics*, in print 2011

[25] Th.M. Wolbank, G. Stojicic, P. Nussbaumer, "Monitoring of Partially Broken Rotor Bars in Induction Machine Drives," *IECON - 36th Annual Conference on IEEE Industrial Electronics Society*, pp.912-917, 2010